Journal of the Korean Physical Society, Vol. 69, No. 7, October 2016, pp. 1225∼1230

Experimental and Theoretical Investigation of the $(In_{0.53}Ga_{0.47}As)_{1-z}(In_{0.52}Al_{0.48}As)_z$ Digital Alloy

Duchang Heo* and Guang-Hoon Kim
Korea Electrotechnology Research Institute (KERI), Ansan 15588, Korea

Jin Dong Song
Korea Institute of Science and Technology (KIST), Seoul 02792, Korea

(Received 20 June 2016, in final form 2 August 2016)

We investigate experimentally and theoretically the band structure of the $(In_{0.53}Ga_{0.47}As)_{1-z}$ $(In_{0.52}Al_{0.48}As)_z$ digital alloy grown by using molecular beam epitaxy as a function of z, where z is defined by the thickness fraction of the InGaAs and the InAlAs layers lattice-matched to InP. To calculate the band structures of the InGaAs/InAlAs digital alloy, we used the 4×4 k·p method; then, we compared these band structures with the photoluminescence experimental results. These experimental and theoretical results show that the InGaAs/InAlAs digital alloy not only can contribute to the method of band-gap engineering by using various types of thickness combinations but also can cover the wavelength gap of 1.2 μm (1.1 μm (GaAs) $< \lambda <$ 1.3 μm (InP)), that only the quantum dot can cover. We also propose a quantum-well structure that is able to cover the wavelength gap.

PACS numbers: 78.30.Fs, 68.65.Cd, 81.07.St
Keywords: Semiconductor, Optical devices, Material growth, Digital alloy
DOI: 10.3938/jkps.69.1225

I. INTRODUCTION

The digital-alloy technique is emerging as a solution for the growth of ternary or quaternary materials of various compositions because it has an advantage of reducing the growth complexity associated with quaternary materials, such as rigorous attention to growth interruption and to the change of source cell temperature, as well as the additional source cell equipment, that is regarded by conventional molecular beam epitaxy (MBE) [1]. In addition, the digital-alloy technique has been used in AlInGaN alloys to increase indium incorporation [2]. The digital-alloy technique is used for growing short-period superlattices (SPSs) with periods of a few monolayers (MLs) of binary or ternary layers by controlling the duty cycle of the constituents during MBE. Since the digital-alloy technique was demonstrated for a laser diode (LD) for the first time to grow an InGaAs asymmetric triangular quantum-well (QW) LD structure [3], Several studies have adapted SPSs grown by using the digital alloy technique to multi-quantum-well (MQW) LDs [4–9]. Recently, an InGaAs/InAlGaAs triangular digital-alloy QW laser structure with an emission wavelength of 2 μm was demonstrated [10–12]. In addition, the concept of a digital alloy has been expanded to photonics and to photonic crystal as well [13]. Several theoretical studies on the optical properties of the digital-alloy InGaAlAs structure have been performed. Its optical properties have been explained by the energy levels of the electrons and the holes confined by an effective barrier made by using an InGaAs/InAsAs digital alloy [1,14].

In this work, to profoundly understand the optical properties of the digital alloy $(InGaAs)_{1-z}(InAlAs)_z$ and the band structure with respect to the composition, z, we theoretically investigate the structure of the digital alloy $(InGaAs)_{1-z}(InAlAs)_z$ by using the 4×4 k·p method, and we compared these results with the experimental data in [1]. We also propose a digital-alloy InGaAs/InAlAs QW structure for a LD covering 1.2 μm of the wavelength gap which only the quantum dot can cover.

II. EXPERIMENT AND THEORETICAL CONSIDERATION

Figure 1 shows a schematic energy-band diagram for the InGaAs/InAlAs digital alloy we investigate, which consists of many pairs of $In_{0.53}Ga_{0.47}As$ and $In_{0.52}Al_{0.48}As$ layers lattice-matched to InP. The In-

*E-mail: dcheo@keri.re.kr; Fax: +82-31-8040-4109

Table 1. Parameter of InGaAs/InAlAs SPSs for the composition (z) of $(InGaAs)_{1-z}(InAlAs)_z$ and the band-gaps (E_g) measured at 300 K and 9 K [1].

Composition (z)	Thickness of $In_{0.53}Ga_{0.47}As$ (Å)	Thickness of $In_{0.52}Al_{0.48}As$ (Å)	E_g (eV) @ 9 K	E_g (eV) @ 300 K
0.2	15	3.75	0.95	0.88
0.4	9.8	6.6	1.10	1.00
0.6	6.6	9.8	1.23	1.19
0.8	3.75	15	1.39	1.34

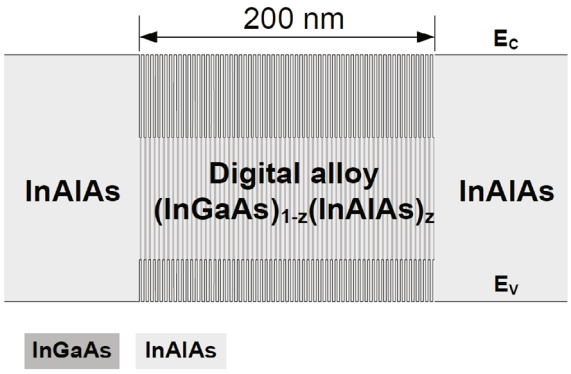

Fig. 1. Schematic illustration of the InGaAs/InAlAs digital alloy lattice-matched to InP. The bandgap can be controlled by the thickness of InGaAs/InAlAs digital-alloy pair. In Table 1, the composition and the corresponding InGaAs/InAlAs digital-alloy pairs are summarized with the optical properties. The total thickness is fixed at 200 nm, and the quantum state is not affected by the outer InAlAs barrier.

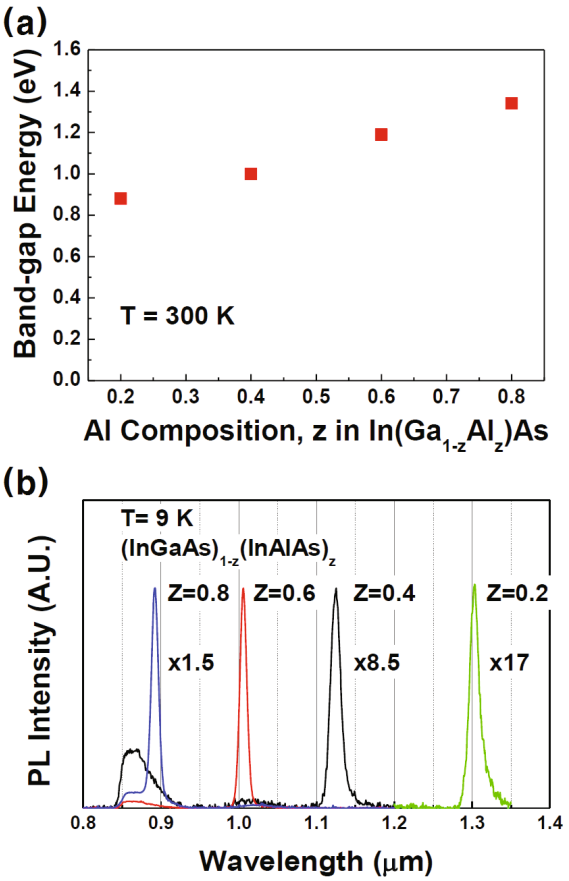

Fig. 2. (Color online) (a) Band-gap energy measured by using PL at room temperature and (b) PL spectra at low temperature for the InGaAs/InAlAs digital alloy.

GaAs/InAlAs layers are grown by using a digital-alloy technique at a temperature of 510 °C in a VG 80H-10K MBE system equipped with compound (GaAs and GaP) decomposition sources for arsenic and phosphorus, respectively. As shown in Fig. 1, the InGaAs/InAlAs digital alloy has a thickness of 200 nm and is surrounded by InAlAs outer barriers. The composition z in the digital-alloy $(InGaAs)_{1-z}(InAlAs)_z$ is defined by the ratio of the thickness of InGaAs to that of InAlAs, and these thicknesses summarized in the Table 1. For example, in the case of $z = 0.2$, the $(InGaAs)_{0.8}(InAlAs)_{0.2}$ digital alloy consists of repeated deposition of 1.5-nm-thick InGaAs layers and of 0.375-nm-thick InAlAs layers, with a thickness ratio of 0.8:0.2 (= 1.5/(1.5 + 0.375): 0.375/(1.5 + 0.375)). We deposit repeatedly the $(InGaAs)_{0.8}(InAlAs)_{0.2}$ digital alloy up to a thickness of 200 nm; therefore, the digital alloy consists of 107 pairs of InGaAs/InAlAs SPSs. In the cases of $z = 0.4$, 0.6, and 0.8, the InGaAs/InAlAs digital alloys consist of 122, 122 and 107 pairs of InGaAs/InAlAs SPSs, respectively. This thickness could be enough to ignore the electron confinement effect due to the InAlAs outer barrier.

Figure 2 shows (a) the band-gap energy measured by using the photoluminescence (PL) peak at 300 K and (b) the 9-K PL spectra of InGaAs/InAlAs digital alloy for $z = 0.2$, 0.4, 0.6 and 0.8. In Fig. 2(b), the small signals around 0.87 um come from the InP substrate. The band-gap energy $E_g(z)$ is observed to vary linearly with z in the range of $z = 0.2$ to 0.8. The linewidths of the InGaAs/InAlAs digital alloy are $10 \sim 15$ meV, which are comparable to those of the InGaAlAs analog alloy.

We used the k·p method within the envelope-function approximation (EFA) to calculate the band structure E(k) of the InGaAs/InAlAs digital alloy with respect to the composition of z by using the finite element method (FEM). The corresponding band-gap energy and wavefunction of the InGaAs/InAlAs digital alloy near the Brillouin zone are also calculated [15]. The total Hamiltonian is $H = H_e + H_h$, and here we ignore the electron-hole coupling, H_{e-h}, due to the high energy-difference between the conduction and the valence bands and the coupling effect between the valence band and the spin-orbit split-off (SO), Δ_0, due to a high energy-separation between them. The coupling effect among two valence bands, heavy hole (HH) and light hole (LH), was consid-

Table 2. Parameters of the InGaAs and InAlAs layers lattice matched to InP.

Parameters	Symbol	(Unit)	$In_{0.53}Ga_{0.47}As$	$In_{0.52}Al_{0.48}As$
Lattice constant	a_0	(Å)	5.8688	5.8688
Band gap at 300 K	E_g	(eV)	0.75	1.45
Average valence band	$E_{v,av}$	(eV)	−6.7875	−7.0636
Spin-orbit splitting	Δ	(eV)	0.3296	0.2998
Electron effective mass	m_e/m_0		0.041	0.075
	γ_1		14.008	12.264
Luttinger parameters	γ_2		5.292	4.6424
	γ_3		6.1061	5.3512

ered, but the strain effect on the InGaAs/InAlAs digital alloy was not considered due to the lattice match to InP. Therefore, the two-band k·p model can be applied and gives a 4 × 4 Hamiltonian matrix, which, together with the corresponding basis functions, is shown below [15]:

$$H^V_{4\times4} = \begin{bmatrix} P_k+Q_k & -S_k & R_k & 0 \\ -S_k^* & P_k-Q_k & 0 & R_k \\ R_k^* & 0 & P_k-Q_k & S_k \\ 0 & R_k^* & S_k^* & P_k+Q_k \end{bmatrix} \begin{matrix} |3/2, & +3/2\rangle \\ |3/2, & +1/2\rangle \\ |3/2, & -1/2\rangle \\ |3/2, & -3/2\rangle \end{matrix}, \quad (1)$$

where

$$P_k = \frac{\hbar^2\gamma_1}{2m_0}(k_x^2+k_y^2+k_z^2) - E_V^0,$$
$$Q_k = \frac{\hbar^2\gamma_2}{2m_0}(k_x^2+k_y^2-2k_z^2),$$
$$R_k = -\sqrt{3}\frac{\hbar^2\gamma_2}{2m_0}(k_x^2-k_y^2) + i2\sqrt{3}\frac{\hbar^2\gamma_3}{2m_0}k_xk_y,$$
$$S_k = 2\sqrt{3}\frac{\hbar^2\gamma_3}{2m_0}(k_x-ik_y)k_z,$$

and m_0 is the free-electron mass, $\hbar$ is the reduced Planck constant, and k_x, k_y, and k_z are wave numbers. The k_z is in the <100> direction. E_V^0 is the valence band edge, which is an important parameter because the probability of the electron and hole distribution in InGaAs/InAlAs SPSs depends on the barrier height of InAlAs in the InGaAs/InAlAs SPSs. The conduction-band offset for InP lattice-matched InGaAs/InAlAs, ΔE_c, is 0.5 − 0.55 eV including interface strain and the transitivity is within 0.01 eV [16]. Here, we chose the conduction-band offset to be 0.5 eV and $dE_c/E_g = 0.714$. In this calculation, we approximate the digital-alloy interface of InGaAs and InAlAs to be an abrupt heterojunction due to the small eigenvalue change caused by surface segregation. R_k^* and S_k^* are the Hermitian conjugates of R_k and S_k. The parameters γ_1, γ_2 and γ_3 are referred to as Luttinger parameters, and are presented in Table 2.

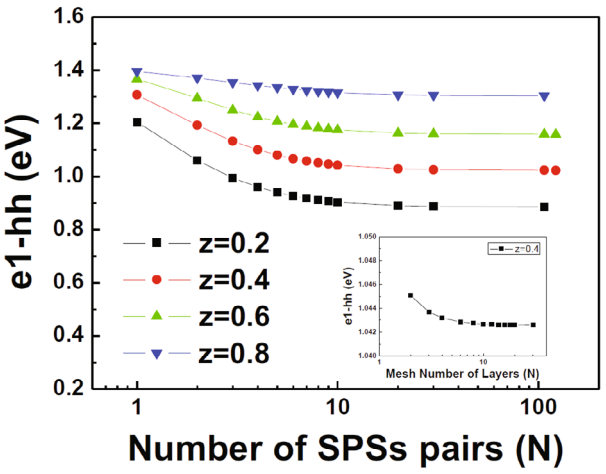

Fig. 3. (Color online) The e1-hh transition energy with respect to the number of InGaAs/InAlAs SPS pairs and z-composition. The transition energy is saturated above 100 pairs of InGaAs/InAlAs SPSs; therefore, the quantum confinement effect due to the outer InAlAs barriers can be ignored. Therefore, the thickness of 200 nm is reasonable for investigating only the effective properties of the InGaAs/InAlAs digital alloy. The inset shows the e1-hh transition energy with respect to the number of meshes of each layer. No change in the transition energy is seen above a mesh number of 15.

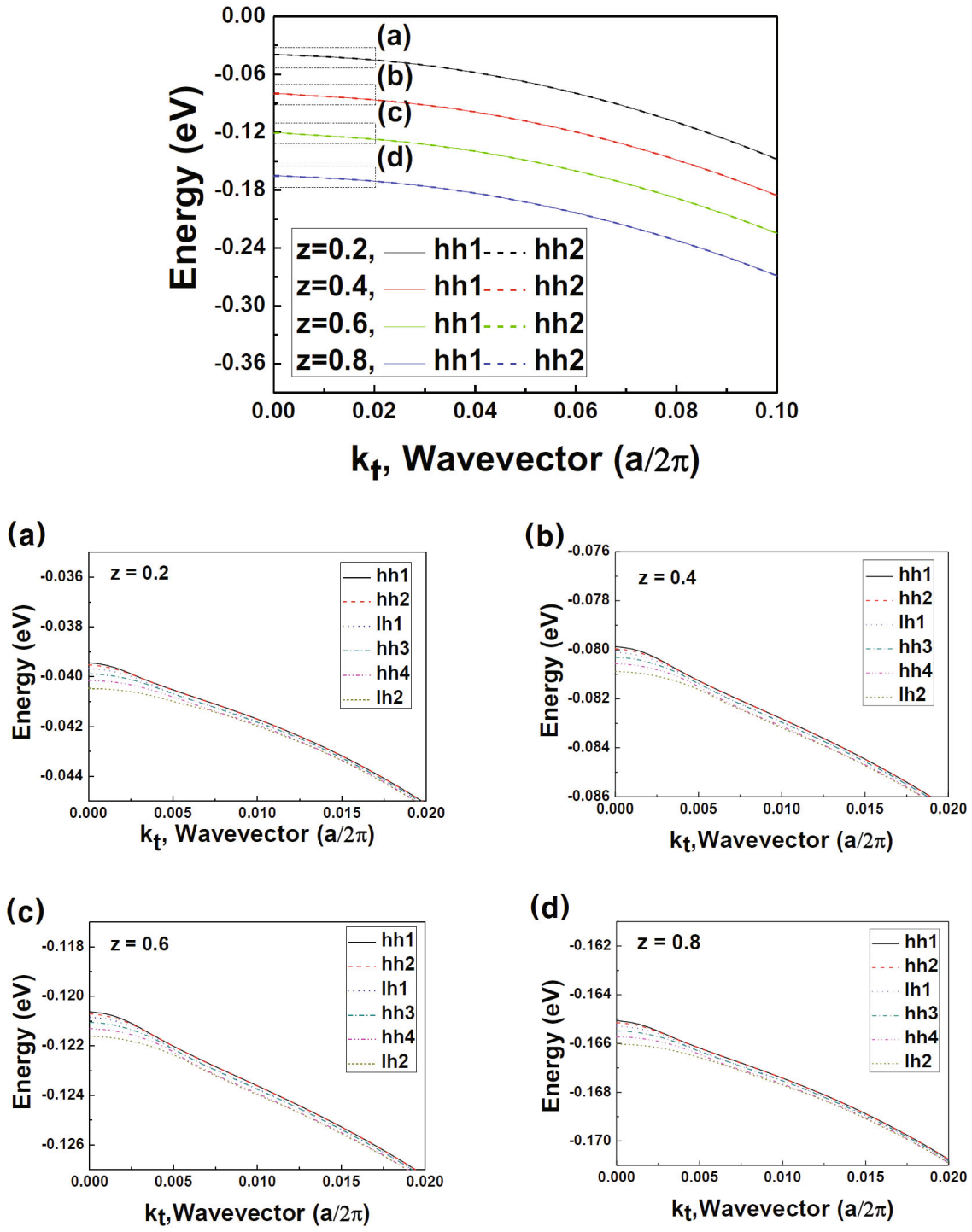

Fig. 4. (Color online) Valence band structure of the InGaAs/InAlAs digital alloy with respect to the z-composition: (a) $z = 0.2$, (b) $z = 0.4$, (c) $z = 0.6$ and (d) $z = 0.8$. The parabolic band structure and split energy of each band can be seen below 1 meV. If we consider the thermal energy, kT, we cannot separate each valence band.

From the Hamiltonian matrix H_{ij} given by Eq. (1), the eigenvalues $E(\vec{k})$ and the corresponding envelope functions of the electrons in the conduction band and the holes in the valence sub-bands can be found by using the FEM to solve the determinant equation.

Figure 3 shows behavior of the e1-hh transition energy with respect to the number of InGaAs/InAlAs SPS pairs and the z-composition at a temperature of 9 K. The transition energies become constant around 100 pairs of InGaAs/InAlAs SPSs, which means that the quan-

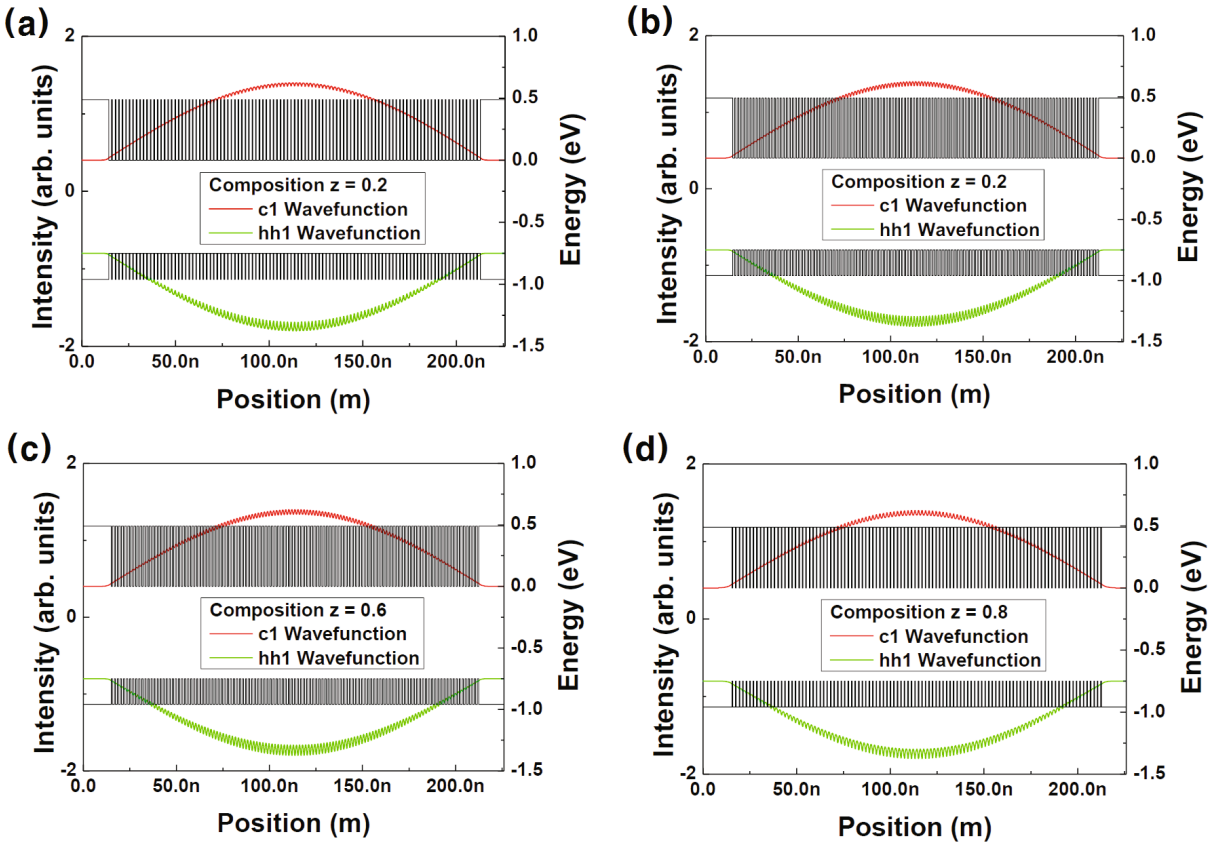

Fig. 5. (Color online) Fundamental electron and hole wavefunctions at $k_t = 0$ with respect to the composition z of the InGaAs/InAlAs digital alloy at room temperature: (a) $z = 0.2$, (b) $z = 0.4$, (c) $z = 0.6$ and (d) $z = 0.8$. The function can be described as a superposition of the carrier distributions of the thin InGaAs well and InAlAs barriers that become the InGaAs/InAlAs digital alloy.

tum confinement effect due to the outer InAlAs barriers can be ignored and that the properties of only the InGaAs/InAlAs digital alloy itself appear with 100 pairs of various combinations of InGaAs/InAlAs SPSs. That is to say, the digital alloy with above 100 pairs of InGaAs/InAlAs SPSs can be described as kinds of bulk-like materials with different energy band-gaps. Therefore, the thickness of 200 nm is reasonable for investigating the effective optical and electrical properties of the InGaAs/InAlAs digital alloy. The inset of Fig. 3 shows the behavior of the e1-hh transition energy with respect to the number of meshes of InGaAs or InAlAs single layers for 200 pairs of InGaAs/InAlAs with $z = 0.4$. The e1-hh transition-energy calculation converges stably above a number of 15 for the single layer. The transition energy converge above a mesh number of 15. Therefore, we used that mesh number to perform the calculation.

III. RESULTS AND DISCUSSION

Figure 4 shows the valence-band structures of the InGaAs/InAlAs digital alloy with respect to the z compositions consisting of about 100 pairs of InGaAs and InAlAs SPSs. Around $k_t = 0$ ($k_t^2 = k_x^2 + k_y^2$), the valence band has a parabolic structure governed by the effective material of the InGaAs/InAlAs digital alloy. In detail, Figs. 4(a)−(d) show valence-band splits caused by the InGaAs/InAlAs barrier, but the split energy is below 1 meV. This value is physically meaningless at room temperature, considering the thermal energy kT. This means that the electron distribution is governed by the effective band structure due to the InGaAs/InAlAs digital alloy.

Figure 5 shows the corresponding wavefunctions of electrons and holes at $k_t = 0$ for the compositions $z = 0.2$, 0.4, 0.6 and 0.8, covering 100 pairs of InGaAs/InAlAs SPSs. The envelope function shows the carrier distribution in the InGaAs/InAlAs digital alloy. This shows a superposition of the electron and the hole distribution functions in the InGaAs wells and the InAlAs barriers of the InGaAs/InAlAs digital alloy. As the composition of z increases, the carrier confinement is relatively and locally strong due to InAlAs barrier's thickness.

Figure 6 shows the calculated emission energy of e1-hh1 with respect to z for the digital alloy $(InGaAs)_z(InAlAs)_{1-z}$ at temperatures of 9 K and 300 K. The emission energy is in good agreement with the

values calculated by using the 4 × 4 band k·p method. However, the values in band-gap calculation are slightly lower than the experimental results. This is attributed to the surface segregation of Ga (Al), which results in an asymmetric gradient of the Ga (Al) mole fraction in the InGaAs/InAlAs interfaces during epitaxy growth [17,18]. However, the In surface segregation, if any, is well known to affect the band gap in the InGaAsP system, but has little of effect on the band gap in the InGaAs/InAlAs SPSs system because the changes in In and As are not at least a mole faction due to similar quantity of the two having been supplied from the MBE sources during growth.

From the above results, we propose a digital-alloy QW structure for LDs using only the InGaAs/InAlAs digital alloy covering around a 1.2-μm wavelength gap (1.1 μm (GaAs) $< \lambda <$ 1.3 μm (InP), which the quantum dot can cover theoretically. Figure 7 shows (a) the e1-hh1 transition wavelength of QWs consisting of a $(InGaAs)_{0.8}/(InAlAs)_{0.2}$ digital-alloy well and $(InGaAs)_{1-z}/(InAlAs)_z$ digital-alloy barrier with $z =$ 0.4, 0.6 and 0.8. Figure 7(b) presents an example of a QW structure and the corresponding band structure with a 1.15-μm emission wavelength consisting of 2 pairs of $(InGaAs)_{0.8}/(InAlAs)_{0.2}$ digital-alloy wells and 7 pairs of $(InGaAs)_{0.2}/(InAlAs)_{0.8}$ digital-alloy barriers. The wavefunction is asymmetric due to the two asymmetric pairs of InGaAs/InAlAs digital-alloy wells.

IV. CONCLUSION

We experimentally and theoretically investigate the band structure of the $(InGaAs)_{1-z}(InAlAs)_z$ digital alloy by using the 4 × 4 k·p method as a function of the z-composition. The calculated results agree well with the peak energy of the PL experiment. The electrons and the holes exist in the InGaAs well and the InAlAs barrier of InGaAs/InAlAs digital alloy. The carrier is tightly confined in the InGaAs well at a high z-composition or a thick InAlAs barrier and is weakly confined at a low z-composition. However, the optical properties are governed by the effective material made of the InGaAs/InAlAs digital alloy. This theoretically and experimentally shows a potentiality for bandgap engineering from 0.855 μm (InGaAs) to 1.563 μm (InAlAs) with only a quaternary of InGaAs and InAlAs by adjusting the number of pairs of the InGaAs/InAlAs digital alloy. Here, we also propose an InGaAs/InAlAs digital alloy QW structure covering 1.2 μm of the wavelength gap (1.1 μm (GaAs) $< \lambda <$ 1.3 μm (InP)), which only a quantum dot can cover theoretically.

ACKNOWLEDGMENTS

This research was supported by Korea Electrotechnology Research Institute (KERI) Primary Research Program through the National Research Council of Science & Technology (NST) funded by the Ministry of Science, ICT and Future Planning (MSIP) (No 16-12-N0101-43).

REFERENCES

[1] J. D. Song, D. Heo, I. K. Han, J. M. Kim, Y. T. Lee and S.-H. Park, Appl. Phys. Lett. **84**, 873 (2004).
[2] L. E. Rodak and D Korakakis, J. Electron. Mater. **40**, 388 (2011).
[3] J. G. Cody, D. L. Mathine, R. Droopad, G. N. Naracas, R. Rajesh and R. W. Carpenter, J. Vac. Sci. Technol. B **12**, 1075 (1994).
[4] F. Schafer, B. Mayer, J. P. Reithmaier and A. Forchel, Appl. Phys. Let. **73**, 2863 (1998).
[5] P. A. Postigo, D. Golmayo, H. Gomez, D. Rodriguez and M. L. Dotor, Jpn. J. Appl. Phys. **41**, L565 (2002).
[6] G. T. Liu, A. Stintz, E. A. Pease, T. C. Newell, K. J. Malloy and L. F. Lester, IEEE Photon. Technol. Lett. **12**, 4 (2000).
[7] N. Ohnoki, G. Okazaki, F. Toyama and K. Iga, Electon. Lett. **35**, 51 (1999).
[8] T. C. Newell, P. M. Varangis, E. Pease, A. Stintz, G. T. Liu, K. J. Malloy and L. F. Lester, Electron. Lett. **36**, 955 (2000).
[9] D. Heo. J. D. Song, I. K. Han, J. I. Lee, J. C. Jenong, J. M. Kim and Y. T. Lee, J. Kor Phys. Soc. **43**, 51 (2003).
[10] Y. Gu, K. Wang, Y.-Y. Li, C. Li and Y.-G. Zhang, Chin. Phys. B **19**, 077304-1 (2010).
[11] Y.-Y. Gao, Y.-G. Zhang, Y. Gu, X.-Y. Chen, L. Zhou and H.-S.-B.-Y. Li, IEEE Photon. Technol. Lett. **26**, 571 (2014).
[12] R. Kaspi, C. Lu, C. Yang, T. C. Newell and S. Luong, J. Cryst. Growth **425**, 5 (2015).
[13] J. Lee, D.-U. Kim and H. Jeon, Opt. Express **19**, 19255 (2011).
[14] B. Kim, K. Kyhm, K. C. Je, J. D. Song, S. Y. Kim, E. H. Le and R. A. Taylor, Curr. Appl. Phys. **14**, 1293 (2014).
[15] J. Piprek, *Semiconductor Optoelectronic Devices* (Elsevier Science, 2003), p. 23.
[16] M. S. Hybertsen, Appl. Phys. Lett. **58**, 1759 (1991).
[17] P. Offermans, P. M. Koenraad, J. H. Wolter, M. Beck, T. Allen and J. Faist, Appl. Phys. Lett. **17**, 4131 (2003).
[18] T. Cresch, *Gain and waveguide engineering in mid-infrared quantum cascade lasers* (thesis of Eth Zurich, 2009), p. 167; G. D. Hong and Y. S. Chang, J. Korean Phys. Soc. **45**, 1000 (2004).